Structure of ultrathin heteroepitaxial superconducting $YBa_2Cu_3O_{7-x}$ films

C. M. Schlepütz,[1,*] M. Björck,[1,†] E. Koller,[2] S. A. Pauli,[1] D. Martoccia,[1] Ø. Fischer,[2] and P. R. Willmott[1,‡]
[1]*Swiss Light Source, Paul Scherrer Institut, CH-5232 Villigen, Switzerland*
[2]*Département de Physique de la Matière Condensée, Université de Genève, Genève, Switzerland*
(Received 5 February 2010; revised manuscript received 12 April 2010; published 20 May 2010)

The atomic structures of ultrathin $YBa_2Cu_3O_{7-x}$ (YBCO) films on $SrTiO_3(001)$ (STO) and $(La_xSr_{1-x})(Al_yTa_{1-y})O_3(001)$ (LSAT) were investigated with sub-Angstrom resolution using surface x-ray diffraction and the phase-retrieval direct-method difference map using the constraints of atomicity and film shift (DCAF). The model-independent electron densities which emerge from random initializations in DCAF are exceedingly stable. The films grow with a well-defined stacking sequence even when grown on substrates with mixed terrace termination. Only very minor out-of-plane deviations from bulk YBCO are observed in the film structures, although they are perfectly strained to the substrate and are therefore tetragonal. The films are superconducting, with critical temperatures for growth on STO and LSAT of 43 K and 70 K, respectively. These results have important implications for reliable structure determination of technologically relevant complex-metal oxide surfaces and interfaces.

DOI: 10.1103/PhysRevB.81.174520 PACS number(s): 74.78.−w, 68.35.−p, 61.05.cp, 81.15.Cd

I. INTRODUCTION

Complex metal oxides (CMOs) exhibit an astonishing wealth of physical phenomena and properties, making them both interesting from a fundamental point of view as well as for their technical applications. These compounds can assume any conduction state from Mott or band-gap insulators via semiconductors and semimetals to high-temperature superconductors.[1–6] The excellent chemical compatibility between many CMO materials not only allows for the specific tailoring of single properties via a controlled change in doping or of the stoichiometry but opens up the opportunity to combine materials with either complementary, competing, or even mutually incompatible characteristics into artificially assembled heterostructures.[7,8]

The unusual effects observable in many CMOs are caused by a complex interplay between the many degrees of freedom in the form of spin, orbit, charge, and lattice interactions caused by strong correlations between the valence electrons. Hence, subtle structural changes in atomic positions can cause wholesale changes in the physical properties of these strongly correlated electron systems (SCESs). Due to the strong ionic bonding in SCESs, distortions induced by, for example, a surface or an interface, typically propagate over distances of several unit cells. In many cases, this implies that the positions of up to a few hundred atoms need to be determined accurately.

To date, only surface x-ray diffraction (SXRD) is capable of determining atomic positions with sub-Angstrom resolution down to depths of several monolayers. Scanning probe techniques, such as scanning tunneling microscopy (STM) and atomic-force microscopy (AFM), provide important localized information, but lack the necessary resolution and the ability to see below the surface layer. Transmission electron microscopy (TEM) does provide depth-sensitive information, but also lacks the required resolution. Furthermore, the samples must be mechanical thinned, which necessarily destroys the specimen (thereby precluding any *in situ* experiments or other subsequent investigations), and also introduces new surfaces, which can themselves effect the structure laterally. Low-energy electron diffraction (LEED) has a resolution which approaches that which is required, although dynamical scattering of the electrons makes quantitative analysis exceedingly difficult. Also, the penetration depth into the sample is very small, and the investigation of buried layers more than a few atomic spacings from the surface becomes impossible.

X rays, on the other hand, interact very weakly with matter and can penetrate deeply into a sample, providing depth-sensitive information for thin films with thicknesses of several nanometers and even reaching buried interfaces. Also, the much simpler kinematical diffraction theory can be applied for quantitative data analysis, and the ultimate resolution far exceeds that obtained with other diffraction techniques. The weak scattered intensities require the use of synchrotron light.

The most severe drawback of all scattering techniques is the phase problem, which prevents a direct determination of the atomic structure based on the measured diffraction intensities alone. Traditionally, this is overcome by using model-refinement procedures. For increasingly complex systems, however, this approach is bound to fail for two simple reasons. First, the correct starting model may not be known *a priori*. Second, the multidimensional "parameter landscape" is liable to contain many local minima, such that finding the global minimum of the true solution represents a formidable task which most standard refinement algorithms cannot fulfill but rather become trapped in local minima in the vicinity of the provided starting guess. Resetting certain parameters and rerunning the fitting routines can help in escaping these minima and obtaining a better goodness of fit although the probability that this represents the global minimum is very small.

There is, therefore, a strong need for an alternative to model-based refinement techniques as the first steps in structure solution. Ideally, the structure should be retrieved without the need to include any detailed knowledge about the atomic composition and arrangements. This can be achieved using direct methods, which have been successfully applied

TABLE I. Structure and properties of the substrates, STO(001) and LSAT(001) in relation to YBCO(001). γ denotes the thermal-expansion coefficient. The YBCO misfit is calculated as $(a-a_{\mathrm{YBCO}})/a_{\mathrm{YBCO}}$ and $(b-b_{\mathrm{YBCO}})/b_{\mathrm{YBCO}}$. "+" denotes tensile strain on YBCO, "–" stands for compressive strain. For LSAT, a simple-cubic structure is assumed.

		Surface unit cell					
Material	Bulk crystal system	a (Å)	b (Å)	Symmetry	Orthorhombicity $\varepsilon=\left\|\frac{a-b}{a+b}\right\|$	YBCO misfit (%) (a/b)	γ $(10^{-6}/\mathrm{K})$
STO(001)	Cubic	3.905	3.905	$p4mm$	0	+2.13/+0.45	9.4
LSAT(001)	Cubic	3.866	3.866	$p4mm$	0	+1.12/−0.54	8.2
YBCO(001)	Orthorhombic	3.823	3.887	$p2mm$	8.37×10^{-3}		10–13

to SXRD (Refs. 9–13) over the past few years. Based only on generic *a priori* physical knowledge of the system (for example, the fact that the electron density should be positive) and the measured diffraction intensities, the corresponding phases can be retrieved using iterative procedures, allowing for a direct reconstruction of the electron density, which may either be interpreted directly or used to construct a well-founded starting model for a subsequent model refinement.

The structure of $YBa_2Cu_3O_{7-x}$ (YBCO) films with thicknesses of a few unit cells is interesting both from a fundamental point of view as well as for the material's use in technical applications. Heteroepitaxial growth of YBCO on different substrate materials induces correspondingly different structural distortions, possibly leading to new and unexpected physical properties.[14] Other interesting questions concern the minimum thickness required to observe superconductivity; the effects of in-plane (e.g., tetragonal) pseudomorphic distortion of the nominally orthorhombic YBCO unit cell on the preferential ordering of the oxygens in the Cu-O chains; and the possibility of oxygen vacancy ordering. For surface-sensitive techniques used to investigate the electronic properties of high-temperature superconductors such as angle-resolved photoemission spectroscopy (ARPES), the detailed atomic arrangement of the topmost atomic layers is of particular interest, in order to decide whether the observed phenomena can be extrapolated to the bulk, or whether one is in fact observing a surface-specific phenomenon.

In this paper, the detailed atomic structures of ultrathin films of YBCO grown heteroepitaxially on $SrTiO_3$ (STO) and $(La_xSr_{1-x})(Al_yTa_{1-y})O_3$ (LSAT) are presented. Both structures are exceedingly bulklike with regards to their out-of-plane atomic positions, though are perfectly tetragonally distorted by the substrates. The films are superconducting. Lastly, the complexity of the presented systems has made them an ideal test bed for investigating the current capabilities and limitations of SXRD in general, and direct methods applied to SXRD in particular. Our results demonstrate the feasibility of solving such a complex structure, containing over 80 atoms (including the top region of the substrate) with picometer accuracy. This result should not be confused with solving three-dimensional crystal structures with unit cells that can contain a far greater number of atoms by single-crystal diffraction. The important difference here is that although there must be an in-plane periodicity equal to an integer multiple of the substrate periodicity, no out-of-plane periodicity is assumed.

II. EXPERIMENTAL

A. Film growth

A summary of the pertinent properties of STO(001) and LSAT(001) in relationship to YBCO is given in Table I. Neither substrate type was chemically prepared before growth, but instead was simply cleaned in acetone then introduced into the growth chamber and heated to the growth temperature of 700 °C.

The miscut of the substrates was less than 0.1°, meaning that terrace widths were larger than 200 nm. Growth was via off-axis magnetron sputtering. Both films were grown simultaneously, ensuring identical conditions. Approximately 4.5 nm of $YBa_2Cu_3O_{7-x}$ were deposited in 1.4×10^{-2} mbar of an $O_2(20\%)/Ar(80\%)$ gas mixture using a stoichiometric, densely pressed YBCO sputter target. After deposition, the samples were slowly cooled to room temperature in 600 mbar of O_2. Finally, a protective cap layer of 10 nm-thick amorphous $PrBa_2Cu_3O_{7-x}$ was deposited at room temperature to minimize both oxygen out-diffusion from the YBCO layer and degradation caused by exposure to ambient conditions.

B. Surface x-ray diffraction

SXRD measurements were performed at the Materials Science beamline X04SA of the Swiss Light Source using 16.000(1) keV synchrotron radiation ($\lambda=0.7749$ Å). The sample was mounted vertically with its surface normal lying in the horizontal plane, and was kept at room temperature and under moderate vacuum ($<10^{-3}$ mbar) inside a small hemispherical beryllium dome. Off-specular CTR data was measured at a fixed incident angle of 0.5°, well above the critical angle for total external reflection of approximately 0.15°. The beam was focused both horizontally and vertically to 0.23 mm(h)$\times$0.84 mm(v). The transverse coherence length parallel to the sample surface was estimated to be approximately 75 nm, that is, at least three times smaller than the substrate terrace width, although the longitudinal coherence length is closer to 1 μm. The relative effect of both of these depends on the orientation of the scattering vector. As we will see, the electron density that emerges does not seem at all smeared out by the coherent addition of parts of the film across a terrace edge, hence we can assume that for the majority of the recorded structure factors the coherently excited volume contained only an insignificant fraction

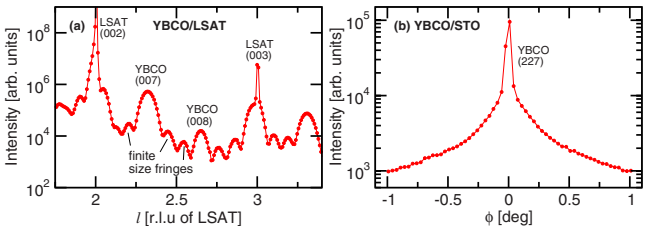

FIG. 1. (Color online) X-ray diffraction measurements on the magnetron sputtered YBCO films. (a) $\theta-2\theta$-scan (b) rocking scan (ϕ-scan) around the YBCO(227) Bragg peak.

of terrace edges. All SXRD data presented here is in units of the substrates' reciprocal lattice units (r.l.u.) of $2\pi/a = 1.6092$ and 1.6252 Å^{-1} for STO and LSAT, respectively.

CTR data sets were recorded for both systems using the PILATUS 100k pixel detector.[15–17] For the chosen x-ray energy, only those CTRs with in-plane indices satisfying $h^2+k^2<26$ could be accessed, and were scanned in l steps of 0.01 r.l.u starting from $l=0.2$ up to the highest reachable point on the CTR. This means that there were approximately eight data points per finite-size fringe [see Fig. 1(a)]. All rods in the first quadrant $(h,k\geq 0)$ of reciprocal space were recorded. However, to investigate systematic effects, a number of randomly selected rods in the remaining three quadrants were also recorded. Unfortunately, the specular $(00l)$ rods were acquired under different experimental conditions, and could not be merged into the final data set. A total of 16 472 (12 184) structure factors on 43 (30) CTRs could be extracted from the YBCO/STO (YBCO/LSAT) data sets and corrected appropriately.

Both data sets were analyzed using the direct method difference map using the constraints of atomicity and film shift (DCAF).[13] An example of four representative rods and the results from a typical DCAF run is shown in Fig. 2.

III. RESULTS

A. Superconducting properties

The superconducting transitions of the YBCO films were measured by inductance measurements. Both films exhibit a reduced critical temperature (T_c) of approximately 43 and 68 K for the ultrathin films grown on STO and LSAT, respectively, compared to the bulk value for optimal doping of $T_c \simeq 91$ K. This is well known for ultrathin films, for which the strain induced by the heteroepitaxial growth makes YBCO

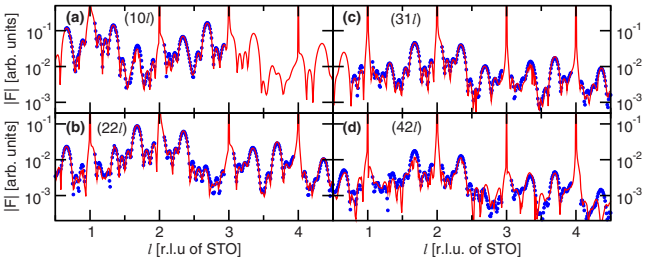

FIG. 2. (Color online) Measured CTRs (circles) plus the output of a typical DCAF run (lines).

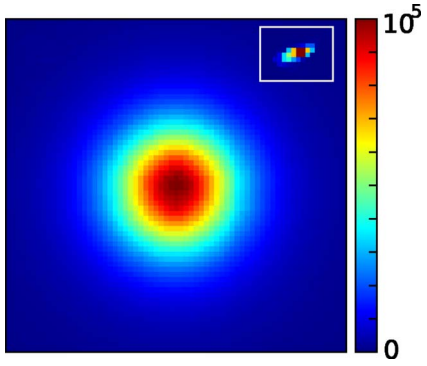

FIG. 3. (Color online) Detector image of the (1/2, 1/2, 1/2) Bragg peak of LSAT, taken without transmission filters. The inset shows a typical integer-order Bragg peak, recorded with a filter transmission of 8.4×10^{-6}, broadened mainly by the large beam footprint on the sample (same spatial and color scales) for comparison.

susceptible to local disruptions from interfaces and defects. Films with a thickness of 30 nm were also deposited on a set of identical substrates. The transitions at 80 and 85 K for growth on STO and LSAT, respectively, are significantly closer to the optimal value, though small differences may suggest a finite-size effect or a marginal underdoping of the material. If only underdoping is responsible, this would correspond to an oxygen content close to 6.7 for which in the bulk material would correspond to an increase in the c-lattice constant from 11.68 to 11.72 Å. If anything, we see a very slight reduction in the lattice constant in the films compared to bulk values, hence it is more probable that finite-size effects are primarily responsible.

B. Diffraction results

Surface superstructures for YBCO grown on STO or for structurally very similar Re $Ba_2Cu_3O_{7-x}$ (Re = rare-earth ion) films have been variously reported.[18–21] No indication of any superstructures could be found on our samples with intensities larger than 0.01 of the weakest parts of the CTR signal.

In this work, we have assumed a simple-cubic structure for the LSAT substrate, with a lattice constant of $a = 3.866$ Å. LSAT actually deviates very slightly from a cubic structure. However, the diffraction data show strong Bragg peaks at all the expected positions for the cubic structure, plus clean CTR signals. The real noncubic structure, characterized by slight distortions, results in a larger unit cell, which produces measurable intensities at half-integer positions in reciprocal space. Figure 3 shows a detector image of such a Bragg peak at (1/2, 1/2, 1/2), proving that such distortions do indeed exist. However, comparing the intensities of these peaks with those corresponding to the simple-cubic structure, we find that the former are weaker by a factor of approximately 10^5. Their broad shape further indicates that the structure of the doubled unit cell is poorly defined. We could observe no signal between these half-integer Bragg peaks along l, proving that they are indeed weak bulk Bragg peaks (and not superstructure rods). The CTR signal in be-

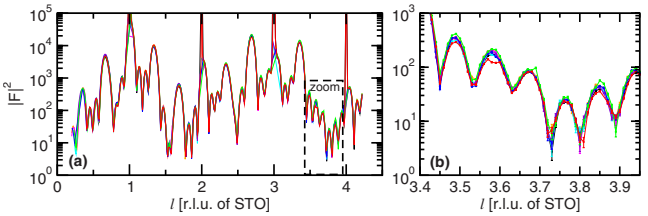

FIG. 4. (Color online) Plot of all eight *p*4*mm*-symmetric CTRs of the (21*l*) family for the YBCO film grown on STO. (a) Overview of the entire CTRs. Significant deviations are visible only at low *l* values. (b) Enlargement of the zoom area marked in the left panel. The systematic errors between the data sets are very small and the statistical uncertainties, as indicated by the error bars, are even smaller and insignificant in comparison.

tween these maxima was unmeasurably weak.

Cubic LSAT(001) and STO(001) have a *p*4*mm* surface symmetry, whereas that of orthorhombic YBCO(001) is only *p*2*mm*. Hence, *a priori*, we might assume that the total symmetry of the substrate-film system would be the lower *p*2*mm*. There are two good reasons why the diffraction pattern should nevertheless be *p*4*mm* symmetric. First, even if we were to assume an orthorhombic YBCO structure, we would expect there to be two orthogonally oriented domains in the film, due to the quadratic surface unit cell of the substrate. In the absence of terrace steps, which are very dilute for the low miscut of the substrates of less than 0.1°, the population of both domains should be equal, resulting in an overall apparent *p*4*mm* symmetry. This was confirmed by a comparison of all the eight CTRs belonging to the (21*l*) family, for both the YBCO/STO and YBCO/LSAT films (Fig. 4).

Second, if the YBCO film is perfectly heteroepitaxially strained to the substrate, the symmetry will be truly, and not just apparently, *p*4*mm*. This was confirmed by an in-plane rocking scan across the (227) Bragg peak of YBCO, plotted in Fig. 1(b). There is no substrate Bragg peak at this position in reciprocal space, so we can be confident that the signal comes from the film. The peak width of less than 0.05° indicates that the domains have in-plane dimensions of at least 65 nm. The sharp peak shape and the absence of any side peaks show that the films are indeed untwinned and perfectly heteroepitaxially strained to match the substrate lattice parameters.

The higher *p*4*mm* symmetry of the film compared to the bulk means that there were a total of 5397 and 5952 independent structure factors on 14 inequivalent rods in an irreducible reciprocal space volume contained in one octant of the in-plane coordinate grid ($0 \leq h \leq 4$ and $0 \leq k \leq h$ for all inequivalent reflections) for STO and LSAT, respectively.

The CTRs exhibit very well-defined finite-size (or "Laue") fringes. The presence of two such fringe maxima in between adjacent YBCO Bragg peaks indicates that the film thickness is very close to the target value of four monolayers (ML).

C. Structural solutions

1. YBCO on STO

Previous SXRD studies on the structure of perovskite substrate-film systems have shown that significant distortions in the substrate are possible down to a few unit cells.[12,22,23] This means that solving the structures of the systems presented here involves finding the positions of roughly 85 atoms (although not all atoms are symmetry independent: first, the *p*4*mm* symmetry does not allow any in-plane movements of the atoms. Second, the $(1/2,0,z)$ and $(0,1/2,z)$ positions are related through a 90° rotation, hence the two atoms must have identical z movements.) If one includes intermixing effects at the interface, partial occupations, and global Debye-Waller factors for each atomic species, this leads to a refinement problem with at least 70 independent parameters, and more than 100 for the more detailed models. As we have already intimated, this represents an enormous challenge for traditional refinement procedures, and bears the inevitable risk of ending up in a local minimum rather than finding the true solution.

To further complicate matters, the choice of starting model is unclear regarding the correct layer stacking at the interface. Chemically, it seems reasonable that the alternate stacking of AO and BO_2 layers in perovskites should prevail across the interface, continuing the network of oxygen octahedra enclosing the small (B) cations. An STO substrate terminated exclusively on the TiO_2 layer would therefore indicate that the first atomic layer of the film should be either BaO or Y. This still allows for three different "B" stacking models of the atomic layers [here, "B" denotes the B-site (TiO_2) terminated domain of the substrate and "|" stands for the nominal interface position]:

(i) B1:
substrate–SrO-TiO_2|BaO-CuO_2-Y-CuO_2-BaO-CuO–⋯.

(ii) B2:
substrate–SrO-TiO_2|BaO-CuO-BaO-CuO_2-Y-CuO_2–⋯.

(iii) B3:
substrate–SrO-TiO_2|*Y*-CuO_2-BaO-CuO-BaO-CuO_2–⋯.

However, the STO substrate used for this study was not chemically prepared for a single termination before growth, meaning that its surface most probably has two types of domain, terminating either on TiO_2 ("B site") or SrO ("A site" termination). Those regions of the substrate surface which are SrO-terminated allow three more possible stacking sequences of the YBCO film:

(i)_ A1:
substrate–TiO_2-SrO|CuO-BaO-CuO_2-Y-CuO_2-BaO–⋯.

(ii) A2:
substrate–TiO_2-SrO|CuO_2-BaO-CuO-BaO-CuO_2-Y–⋯.

(iii) A3:
substrate–TiO_2-SrO|CuO_2-Y-CuO_2-BaO-CuO-BaO–⋯.

Note that if the SrO-terminated domain lies one atomic layer (i.e., half a unit cell) *above* the TiO_2-terminated surface, there will be the same stacking of the YBCO as one travels in the film plane across the stacking-sequence combinations B1/A3, B2/A1, and B3/A2. If the A-site termination lies half a unit cell *below* the B-site termination, the same is true for the combinations B1/A1, B2/A2, and B3/A3 (see Fig. 5). If a significant fraction of stacking-pairs other than one of these six were present, the resulting electron-density map would be smeared, both regarding the atomic positions in the z direction, and also the atoms' integrated electron densities. Indeed, as we shall see, all the direct-method analyses produced only the B1/A1 combination.

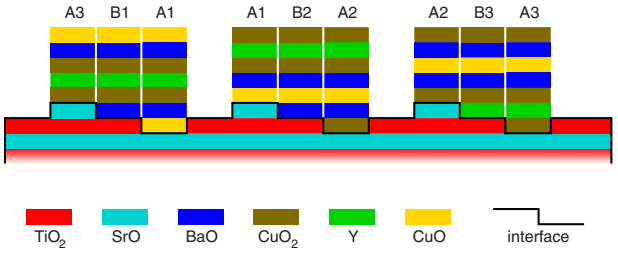

FIG. 5. (Color online) The six considered stacking sequences A1–A3 and B1–B3 of YBCO on $SrTiO_3$ shown in the different lateral combinations which produce the same in-plane chemistry in the film.

Initial attempts to retrieve an unambiguous structure using coherent Bragg rod analysis (COBRA) (Ref. 9) were unsuccessful. COBRA requires an approximate model of the substrate-film structure as a starting point for the iterative phase-retrieval process. The two stacking sequences A1 and B1 were used in two independent runs as the starting reference structures, and in both cases, the COBRA output retained the YBCO film termination layer given by the starting models (BaO and CuO, respectively), while the interfaces were clearly different regarding the electron densities. Both results yielded comparable *R* factors of approximately 5%, so could not be used as a guide. At least one of these solutions must be wrong, however. It was therefore concluded that COBRA alone cannot unequivocally determine the stacking sequence and surface termination in YBCO/STO.

DCAF, on the other hand, is seeded with randomly generated electron densities, allowing for multiple independent restarts of the structure solution, rendering it effectively model independent. Hence, our confidence in the validity of a model increases if it consistently emerges from several DCAF runs.[13] The tradeoff for this increased reliability lies in the slower convergence of the algorithm, typically requiring a few thousand iterations, running between 30 and 180 min on a standard computer.

The raw output from ten DCAF runs is shown in Fig. 6(a), after optimization of the real-space support constraint and the threshold for recognition of atomicity (these are essentially the only two aspects of DCAF which can be considered to introduce an element of model dependence, although this is very weak[13]). The *R* factor for the ten runs ranged from 9.5% to 11.3%. The reason that these values are generally higher than those obtained in COBRA is that in DCAF the strong constraint of atomicity is used, which forbids the formation of electron-density "grass."

The line scans contain stable peaks at the predicted lattice spacing for an YBCO-like structure and show the expected ordering. It is again stressed that these peaks emerged from a *random* electron-density distribution, only by enforcing a few real-space constraints and using the measured diffraction intensities. In no way were the expected positions of these peaks included in the algorithm. In other words, DCAF does not know we are looking for YBCO.

The scatter between the ten solutions gives an indication for the reliability of the retrieved structures. For example, the

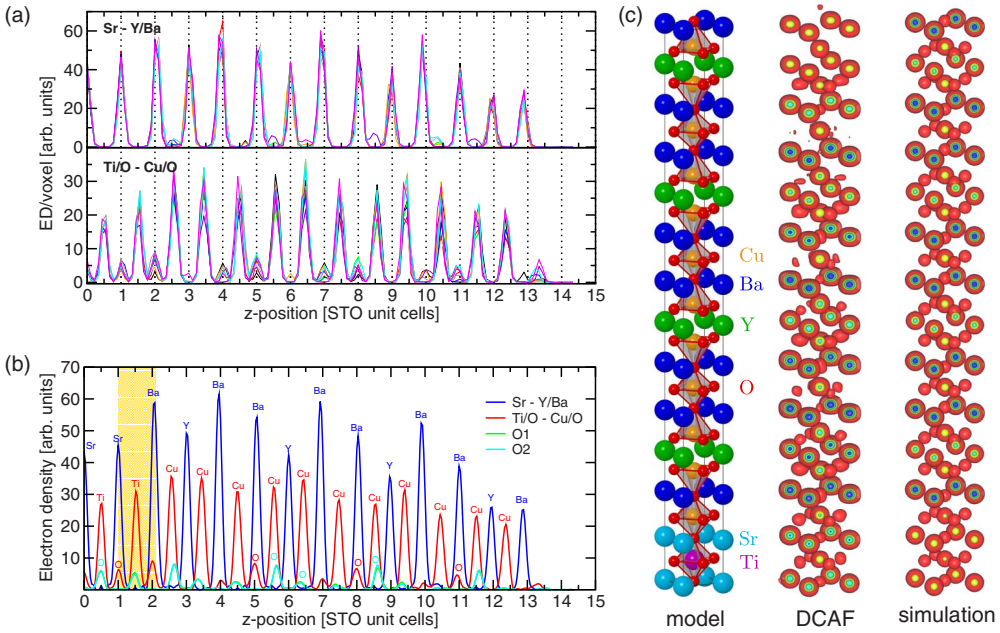

FIG. 6. (Color online) (a) Comparison of the results obtained from ten DCAF runs. The two panels show the line plots of the retrieved electron density along the out-of-plane direction through atomic rows of Sr–Ba/Y (top) and Ti/O–Cu/O (bottom). The support regions, equal to 15 unit cells of STO in height, are large enough to contain the equivalent of four unit cells of YBCO and two of STO. (b) The averaged and artificially ×3 upsampled electron-density line-profiles from ten phase-retrieval runs. Four lines through the high-symmetry in-plane positions of the bulk STO reference structure are shown. The tentative assignment of atom types, based on a bulklike YBCO film on STO, is indicated above the peaks (not all oxygens are labeled). The yellow band marks the range of the interface. (c) DCAF result compared to a bulklike YBCO structure on STO. Left: ball-and-stick model of a bulklike structure with sharp interface; center: isosurfaces of the DCAF retrieved ED map; and right: isosurfaces of a simulated ED map based on the ball-and-stick model. Note that both possible orientations of the oxygen atoms in the CuO planes are shown simultaneously and therefore have an occupation factor of 0.5.

seven small peaks in the upper panel of Fig. 6(a) only appear in very few runs and are very probably artifacts. In contrast, on the Ti/O-Cu/O lines (bottom), the small peaks correspond to oxygen atoms in the YBCO unit cell. Although they are missing for some of the results, their occurrence is much higher than for the small peaks in the upper panel. Note also that in the lower panel, they occur with high probability periodically for two out of three positions, corresponding to the known oxygen ordering in YBCO (there is no oxygen in the yttrium layers). The uncertainty in the ED map therefore seems to be on the level of these small peaks, meaning that the sensitivity limit is of the order of a few oxygens for the entire structure comprising over 75 atoms. The presence and positions of the heavy ions are exceedingly stable in all ten runs. Moreover, even for the oxygen atoms in the CuO_2 planes that sandwich the Y atoms, a consistent displacement toward the Y layer is clearly observed, while those oxygens in the BaO layers move toward the CuO plane, as found in bulk YBCO.

The resolution of the electron density is determined by the maximum momentum transfer of the diffraction data. The first model of the atomic structure from the DCAF solutions was obtained from the average of all ten ED maps. This enhances the consistent peaks while suppressing spurious features. Visually, an artificial upsampling of the ED is very helpful, and does not introduce artifacts if performed only at the end of the analysis. A plot of the averaged and upsampled ED lines is displayed in Fig. 6(b). They are remarkably similar to what one would expect when assuming that the film has the known structure of bulk YBCO but is pseudomorphically strained to the substrate's in-plane lattice constants, except in two cases. First, the oxygen peak in the topmost BaO-layer is missing. This is almost certainly caused by the partial occupation of the topmost monolayer. It seems highly unlikely that the oxygen is really missing here, as this would be both chemically and electrostatically highly unfavorable. Second, it remains ambiguous as to whether the STO interface is TiO_2 or SrO terminated. This may well be because the termination is not unique. Importantly, however, the YBCO-surface seems to be clearly BaO terminated, which, surprisingly if one assumes stoichiometric block-for-block growth, speaks more for an SrO-terminated STO substrate. Finally, it should be mentioned that, from the ED map alone, we cannot distinguish between atoms of similar Z such as Sr and Y or Cu and Ti, and have relied on the bulk structures of both YBCO and STO to guide us here. Also at the surface and importantly at the interface, we cannot easily disentangle partial occupation from atom type (in other words, is a site 100% Ti or 76% Cu occupied, or indeed a mixture of these, as they all have the same integrated number of electrons). In our interpretation we have made the two assumptions that the atom sites at the interface are 100% occupied but can be intermixed, while those sites at the surface contain only one atom type but might be only partially occupied.

The atomic positions emerging from the averaged DCAF runs were determined by fitting the electron-density peaks to three-dimensional Gaussians, which also yielded the atomic widths (i.e., the Debye-Waller factors). The $p4mm$ symmetry of the structure prohibits any in-plane movements of atoms. Therefore, the observed shifts in the x and y directions

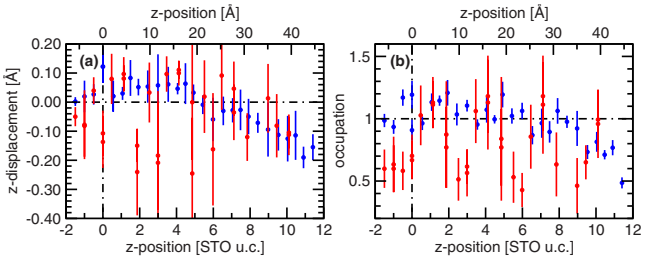

FIG. 7. (Color online) Quantitative DCAF results, shown for the reliably identified heavy atoms (Sr, Y, Ba, Cu, and Ti shown in blue) and the more unstable oxygen atoms (red). The vertical dashed line marks the position of the nominally first YBCO layer above the interface. (a) Atomic displacements in the z direction with respect to a bulklike YBCO structure. (b) Calculated occupation of the atomic sites as a function of depth.

should be all zero. However, in DCAF, this symmetry constraint is not applied directly in real space to the retrieved ED, but only indirectly through the corresponding symmetrization of the diffraction pattern. The observed shifts can therefore give a direct estimate about the approximate accuracy of the calculated peak positions. These lie in the range of 2 pm.

The spread in the z positions are only moderately larger than that in x and y, having an rms deviation of approximately 8 pm, which means that the positions should be interpreted cautiously. Figure 7 shows both the atomic shifts in the z-direction and the calculated occupation for each site for the entire film when compared to bulk YBCO ($c=11.68$ Å) on STO ($c=3.9045$ Å). The occupations are calculated based on the assigned atom type and the integrated electron density in the corresponding peaks. Since the composition at the interface due to intermxing is not exactly known, the corresponding occupancy parameters, which are based on the assignment of only one atom type, have therefore to be interpreted with care. As mentioned above, for further analysis, we have postulated a 100% occupancy instead and have thus determined the intermixing ratio of the different atomic species. The variations in the values obtained for oxygen are at approximately ± 0.2 fairly large, and may not be purely due to statistical fluctuations. One likely source of error is the absolute scaling of the experimentally determined structure factors, which determines the total electron density of the system. A scale factor which is too large will likely result in an overestimation of the atomic occupations, while small shifts in electron density from one atom to another will have a larger impact on the low-Z oxygen than on the heavy cations.

The displacements along z are small, but there does seem to be a consistent and statistically significant dilation of the heavy-ion lattice in the first two YBCO unit cells, followed by a slight compression in the topmost layers toward the surface. The effect is very small, however, as the total displacement at the surface corresponds to approximately 0.16 Å over a film thickness of nearly 45 Å.

Finally, Fig. 6(c) shows a plot of DCAF-generated three-dimensional electron-density isosurfaces next to a ball-and-stick model of bulk YBCO and the simulated isosurfaces based on the bulk model. The ball-and-stick model and the

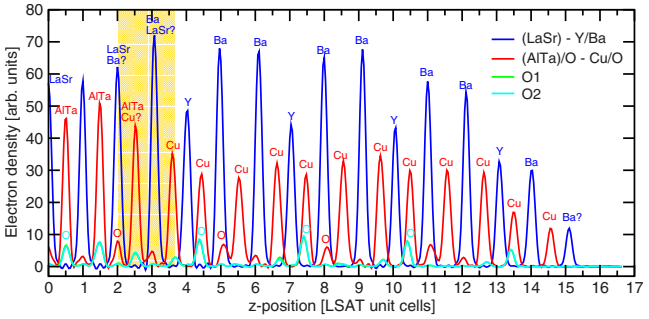

FIG. 8. (Color online) Averaged and artificially ×3 upsampled ED line-profiles from ten optimized DCAF runs of YBCO on LSAT. Four line cuts through high-symmetry points of the in-plane structure are shown. The yellow band marks the approximate position of the interface between YBCO and LSAT. Assignments of the atomic species are shown above the peaks.

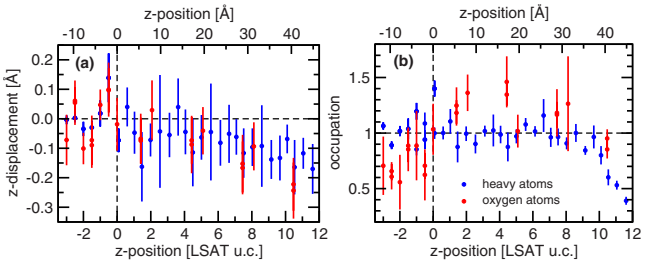

FIG. 9. (Color online) Results of a quantitative analysis of the DCAF results. The values for heavy atom are shown in blue, and those for the oxygen atoms in red. (a) Atomic displacements in the z direction with respect to a bulklike LSAT-YBCO reference structure. (b) Calculated occupations of the atomic sites as a function of depth.

simulation are shown with a CuO_2 layer (as against CuO) in between the BaO layers. The average occupancy of each of the O atoms in this layer is therefore 50%. Indeed, closer inspection of the three-dimensional isosurface and the CuO positions in Figs. 6(b) and 7(b) shows that the occupancy of these O atoms is approximately 0.5 (although some of the other O-atom occupancies are also well below unity and are associated with large error bars). Overall, the degree of agreement is very impressive, validating DCAF as a successful phase-retrieval technique, and also demonstrating the bulklike nature of the YBCO film.

From the DCAF results, the cationic positions are known with an accuracy of the order of ±4 pm, while the oxygen positions have a mean accuracy of ±8 pm. The occupations and widths have also been estimated (albeit with more uncertainty). Based on this, a first structural model can be proposed, and used as a basis for further analysis. For this, different combinations of COBRA,[9] FIT,[24] and GenX (Ref. 13) were employed. Details of the different strategies can be found elsewhere.[25] The essential results obtained from the earlier DCAF analysis remained unchanged, although more accurate information was gleaned. In addition to the determination of the stacking sequence down to the two homologs A1 and B1, the refined atomic positions consistently indicate a slight compression of the YBCO film unit cell of less than 1% compared to the bulk lattice constant for optimal doping of 11.68 Å. The high crystalline quality of the film is confirmed by very modest Debye-Waller factors of around 1.0 for the substrate atoms at the interface and approximately 2.5 for the film atoms. Lastly, a consistent value for the occupation of the uppermost unit cell of YBCO of approximately 80% was determined. Although not physically relevant in itself, it is reassuring that the different refinement strategies in this last stage produced mutually compatible results.

2. YBCO on LSAT

The procedure for determining the structure of YBCO on LSAT followed that described above for the YBCO/STO system. The averaged results from ten DCAF runs (R factors ranging from 9.7% to 10.7%) are shown in Fig. 8. The atomic arrangement again corresponds exactly to what would be expected for YBCO. Most oxygen atoms are also present, apart from in the topmost atomic layers and, again, in the CuO layers, where the enforced $p4mm$ symmetry means that the CuO chains have no preferred in-plane direction, resulting in an occupancy of 0.5 for these O atoms. This brings their electron density below the threshold for the atomicity constraint in DCAF. The transition from the LSAT substrate to the YBCO film at the interface is more gradual than for STO/YBCO and occurs over some four atomic layers. The terminating layer at the surface consistently shows an additional small peak at a nominal Ba site on top of complete YBCO unit cell terminated on the CuO chain layer, suggesting the possibility of a BaO overlayer at the surface. The corresponding oxygen peaks would be too weak to be observed, due to the strong drop off effect at the surface caused by the window function in DCAF.

The results of a quantitative analysis of the peak positions in the ED map are shown in Fig. 9. Only those values are plotted for which the ED peak could be unambiguously identified in at least five out of the ten randomly initialized DCAF runs (note the missing oxygens as a result). The z displacements exhibit again a slight contraction with respect to a bulklike YBCO unit cell, although this has error bars produced by the scatter of the positions from run to run that are almost as large as the contraction. Otherwise, no significant atomic movements are visible.

IV. DISCUSSION

The first important result is the electron density produced by DCAF. The positions of the heavy atoms, along with the narrowness of the features, emerge consistently and unambiguously from many independent DCAF runs starting with random "foglike" electron densities. Although other methods such as reflection high-energy electron-diffraction (RHEED),[26] x-ray standing waves (XSW),[27] atomic-force microscopy,[28] and scanning-tunneling microscopy and spectroscopy (STM/STS) (Ref. 29) have provided important clues about the nucleation and stacking of YBCO thin films, as far as the authors are aware, this is the first direct determination of all atomic positions with picometer accuracy over the entire film and substrate interface thickness of over 5 nm.

The structural model for the STO/YBCO system emerging from our analysis is summarized as follows: from the narrowness of the ED-peaks and their positions, which so accurately resemble bulk YBCO, we can be sure that the film structure above the interfacial region is well defined and constant across the whole film surface. Comparison of the ED maps in Fig. 6(b) with the schematic stackings shown in Fig. 5 shows that stacking is based on the A3/B1/A1 triplet.[28,30] Because the x-ray coherence length of approximately 75 nm is considerably smaller than the terrace width, the ED maps have only insignificant contributions from signal originating for coherent scattering across terrace edges. This is further supported by the equivalence of the eight CTRs shown in Fig. 4; because the terraces have a well-defined in-plane orientation, these CTRs would differ from one another if the signal originating across the terraces were significant.

Note that the A1 stacking sequence begins the film with CuO, and we would therefore expect the O atom at this position [at 1.5 on the x axis is Fig. 6(b)] to be smaller due to the occupancy of 0.5, which, within the experimental accuracy, we believe we do not observe. One might thus speculate that the A3/B1 sequence pair is more probable than B1/A1, though this is far from certain.

The averaged structure over the different substrate termination domains within a given terrace results in an apparent SrO/BaO intermixing at the interface, observable in the ED maps as a transition over approximately two atomic layers. This cannot be an artifact produced by an apparent roughness caused by the terraces, as all other atomic layers of the structure above the interface remain in exact registry when traversing from one substrate termination domain to another (within any given terrace). The surface termination of the film grown on STO was found to be predominantly on the first BaO layer following the Y planes.

As one traverses a terrace edge, the YBCO stacking shifts with the terrace step and hence there must be a grain boundary formed. This is in contrast to the growth configuration proposed by Zegenhagen *et al.*[27] There, it was suggested that as one moves up a terrace edge of STO, this vertical shift of 3.9 Å is accommodated by the YBCO film stacking sequence starting at the next "subunit" of the YBCO unit cell higher up, whereby the three subunits consist of $BaCuO_{2.5}$-$YCuO_2$-$BaCuO_{2.5}$. The ED maps presented here clearly do not show this, as this would result in significant smearing of the peaks and an averaging of their heights.

Hence, exactly at the terrace edges, there will be considerable vertical strain and the formation of grain boundaries: the height of the $BaCuO_{2.5}$ subunit is, at 4.14 Å, 0.55 Å greater than that of the $YCuO_2$ subunit. Despite the energy that this must cost, it seems to be lower than that associated with changing the start of the YBCO stacking sequence to accommodate the terrace step. A possible reason for the apparent contradiction between these results and those of Zegenhagen *et al.* is that we use substrates with very low miscuts. As the terrace-edge density is proportional to the miscut angle, the stacking-fault energy at the terraces for a film only containing the A3/B1/A1 stacking sequence triplet will increase with miscut angle. Above a critical value, the mixed "terrace-edge-matching" stacking-sequence proposed by Zegenhagen will presumably be favored.

On the atomic level, the out-of-plane film structure remains exceedingly bulklike. Assuming the limiting case of an ideal Poisson ratio of 0.5, i.e., a constant volume of the unit cell, the compression resulting from the in-plane tensile strain would be approximately 2.5 %. The observed c-axis reduction of slightly less than 1% is in excellent agreement with the reported Poisson ratio for YBCO of 0.17.[31] Unfortunately, the final sensitivity to detect changes in the oxygen positions or occupations was found to be insufficient to make any conclusive statements about these aspects.

Analysis of the LSAT/YBCO system has provided a general picture of the global film structure with high confidence. The DCAF solution, based only on *a priori* information and the measured structure factors, gives an excellent and model-independent confirmation for the correct atomic structure and the high quality of the heteroepitaxially grown YBCO film. The sensitivity to detect more subtle changes on the atomic level with high precision is insufficient, however, to determine the exact interfacial structure, the distribution of oxygen atoms within the film, and the structural changes induced by the symmetry and strain of the substrate.

The forced increase in symmetry of the YBCO film has important consequences for its structure. A prominent feature of bulk YBCO is the CuO chain along the crystallographic b direction, separated by oxygen voids in the a direction. This in-plane directionality disappears with the biaxial pseudomorphic straining of the film, however. Unfortunately, the present analysis can give no information of the lengths of any CuO chains that might be present. The pseudomorphic strain in the b-axis direction between YBCO and STO is only 0.45% and is tensile, while that between YBCO and LSAT is 0.54%, but is compressive (see Table I), which may explain the higher critical temperature of films grown on LSAT compared to those on STO.[14,32,33]

This detailed structural information about the films is important for other investigations. First, it provides a firm structural basis for the interpretation of surface-sensitive measurements, for example of the electronic structure using angle-resolved photoelectron spectroscopy. Second, it may serve as a well-defined and realistic starting point for theoretical models, as for instance for band-structure calculations. Finally, the fact that the film structure is quasibulklike allows for a direct correlation between bulk properties and experimental results obtained from high-quality thin-film samples, making them viable substitutes for bulk samples, where the latter are unavailable in sufficient quality.

V. CONCLUSIONS

In conclusion, the structure of ultrathin YBCO films grown pseudomorphically on STO and LSAT have been determined in a model-independent fashion using the phase-retrieval direct method DCAF. This is the most complex system to be analyzed using DCAF or similar phase-retrieval techniques and one of the most complex systems to be solved using SXRD in general. The atomic out-of-plane (z) positions which emerge from the DCAF analysis, which, remember, uses no model input, are so extremely close to bulk values for YBCO that this system can in hindsight be con-

sidered to be an excellent test bed for the efficacy of DCAF as a structural solution algorithm, which can provide a basis for still more sophisticated structural analysis.

The emerging electron densities show that the films grow with only one main stacking sequence ("B1") on top of the B-site terminated parts of the substrate (TiO_2 for STO and Al/TiO_x for LSAT), with additional contributions (A1 and A3) from those regions of the substrate terminating one atomic layer below and above on the A site of the substrate. These merge perfectly with the B1 sequence above the interface. There might also be marginal intermixing at the substrate over approximately three atomic layers, although it is hard to distinguish this from mixed termination effects.

Apart from the forced tetragonal symmetry of the films produced by the pseudomorphic growth, they shows an exceedingly bulklike structure, with a marginal compression out of plane of approximately 1% in the case of growth of YBCO. This provides vital information and a firm structural basis for the interpretation of heteroepitaxial interfacial structures of YBCO with other technologically relevant systems such as the colossal magnetoresistive manganites.

For the present state-of-the-art SXRD analysis, the accurate determination of the positions and occupations of low-Z materials as oxygen is still very challenging. Ultimately, however, one would like to be sensitive to small movements and partial occupations of these atoms. This will set stringent requirements on the accuracy of both the measurements and also the employed direct methods and model-refinement tools.

ACKNOWLEDGMENTS

The authors would like to thank Yizhak Yacoby for fruitful discussions. Support of this work by the Schweizerischer Nationalfonds zur Förderung der wissenschaftlichen Forschung and the staff of the Swiss Light Source is gratefully acknowledged. This work was partly performed at the Swiss Light Source, Paul Scherrer Institut.

*Present address: Department of Physics, University of Michigan, 450 Church Street, Ann Arbor, MI 48109-1040, USA.
†Present address: MAX-lab, Lund University, P.O. Box 118, SE-221 00 Lund, Sweden.
‡philip.willmott@psi.ch

[1] J. G. Bednorz, and K. A. Müller, Z. Phys. B: Condens. Matter **64**, 189 (1986).
[2] S. Jin, T. Tiefel, M. McCormack, R. Fastnacht, R. Ramesh, and L. Chen, Science **264**, 413 (1994).
[3] M. B. Salamon and M. Jaime, Rev. Mod. Phys. **73**, 583 (2001).
[4] C. Ahn, K. Rabe, and J.-M. Triscone, Science **303**, 488 (2004).
[5] D. Fong, G. Stephenson, S. Streiffer, J. Eastman, O. Auciello, P. Fuoss, and C. Thompson, Science **304**, 1650 (2004).
[6] M. Dawber, K. M. Rabe, and J. F. Scott, Rev. Mod. Phys. **77**, 1083 (2005).
[7] A. Ohtomo and H. Y. Hwang, Nature (London) **427**, 423 (2004).
[8] E. Bousquet, M. Dawber, N. Stucki, C. Lichtensteiger, P. Hermet, S. Gariglio, J.-M. Triscone, and P. Ghosez, Nature (London) **452**, 732 (2008).
[9] Y. Yacoby, R. Pindak, R. MacHarrie, L. Pfeiffer, L. E. Berman, and R. Clarke, J. Phys.: Condens. Matter **12**, 3929 (2000).
[10] D. K. Saldin, R. J. Harder, V. L. Shneerson, and W. Moritz, J. Phys.: Condens. Matter **13**, 10689 (2001).
[11] L. D. Marks, N. Erdman, and A. Subramanian, J. Phys.: Condens. Matter **13**, 10677 (2001).
[12] P. R. Willmott, S. A. Pauli, R. Herger, C. M. Schlepütz, D. Martoccia, B. D. Patterson, B. Delley, R. Clarke, D. P. Kumah, C. N. Cionca, and Y. Yacoby, Phys. Rev. Lett. **99**, 155502 (2007).
[13] M. Björck, C. M. Schlepütz, S. A. Pauli, D. Martoccia, R. Herger, and P. R. Willmott, J. Phys.: Condens. Matter **20**, 445006 (2008).
[14] J.-P. Locquet, J. Perret, J. Fompeyrine, E. Mächler, J. W. Seo, and G. V. Tendeloo, Nature (London) **394**, 453 (1998).
[15] A. Bergamaschi, Ch. Brönnimann, E. F. Eikenberry, B. Henrich, M. Kobas, P. Kraft, and B. Schmitt, PoS **57**, 049 (2007).
[16] P. Kraft, A. Bergamaschi, C. Brönnimann, R. Dinapoli, E. F. Eikenberry, H. Graafsma, B. Henrich, I. Johnson, M. Kobas, A. Mozzanica, C. M. Schleputz, and B. Schmitt, IEEE Trans. Nucl. Sci. **56**, 758 (2009).
[17] P. Kraft, A. Bergamaschi, Ch. Brönnimann, R. Dinapoli, E. F. Eikenberry, B. Henrich, I. Johnson, A. Mozzanica, C. M. Schlepütz, P. R. Willmott, and B. Schmitt, J. Synchrotron Radiat. **16**, 368 (2009).
[18] M. Alario-Franco, C. Chaillout, J. J. Capponi, J. Chenavas, and M. Marezio, Physica C **156**, 455 (1988).
[19] X. Torrelles, C. Aruta, A. Fragneto, I. Maggio-Aprile, L. Ortega, F. Ricci, J. Rius, M. Salluzzo, and U. Scotti di Uccio, Phys. Rev. B **70**, 104519 (2004).
[20] D. J. Werder, C. H. Chen, R. J. Cava, and B. Batlogg, Phys. Rev. B **37**, 2317 (1988).
[21] H. Behner, K. Rührnschopf, W. Rauch, and G. Wedler, Appl. Surf. Sci. **68**, 179 (1993).
[22] R. Herger, P. R. Willmott, O. Bunk, C. M. Schlepütz, B. D. Patterson, and B. Delley, Phys. Rev. Lett. **98**, 076102 (2007).
[23] R. Herger *et al.*, Phys. Rev. B **77**, 085401 (2008).
[24] O. Bunk, Ph.D. thesis, University of Hamburg, 1999.
[25] C. M. Schlepütz, Ph.D. thesis, University of Zürich, 1999.
[26] T. Terashima, Y. Bando, K. Iijima, K. Yamamoto, K. Hirata, K. Hayashi, K. Kamigaki, and H. Terauchi, Phys. Rev. Lett. **65**, 2684 (1990).
[27] J. Zegenhagen, T. Siegrist, E. Fontes, L. E. Berman, and J. R. Patel, Solid State Commun. **93**, 763 (1995).
[28] V. C. Matijasevic, B. Ilge, B. Stäuble-Pümpin, G. Rietveld, F. Tuinstra, and J. E. Mooij, Phys. Rev. Lett. **76**, 4765 (1996).
[29] T. Haage, J. Zegenhagen, H.-U. Habermeier, and M. Cardona, Phys. Rev. Lett. **80**, 4225 (1998).
[30] R. Ramesh, A. Inam, D. M. Hwang, T. S. Ravi, T. Sands, X. X. Xi, X. D. Wu, Q. Li, T. Venkatesan, and R. Kilaas, J. Mater. Res. **6**, 2264 (1991).
[31] B. Bridge, J. Mater. Sci. Lett. **8**, 695 (1989).
[32] L. Gao, Y. Y. Xue, F. Chen, Q. Xiong, R. L. Meng, D. Ramirez, C. W. Chu, J. H. Eggert, and H. K. Mao, Phys. Rev. B **50**, 4260 (1994).
[33] L. X. Cao, J. Zegenhagen, E. Sozontov, and M. Cardona, Physica C **337**, 24 (2000).